SIMULATING CRISM IMAGES: A TOOL FOR RESEARCHERS IN TESTING AND CONFIRMING GEOLOGIC ANALYSES OF CRISM IMAGES OF MARS. M. Parente[1, 2], J. T. Clark[2], J. L. Bishop and A. J. Brown[2], [1]Department of Electrical Engineering, Stanford University, Stanford, CA, 94305 (Mario.Parente@stanford.edu), [2]Carl Sagan Center, SETI Institute, Mountain View, CA, 94043.

Introduction: Automated analysis of hyperspectral remote sensing data of the Martian surface is challenging due to a lack of ground truth for most regions of the planet and incomplete knowledge of the atmospheric and geologic variables. Modeling the remote sensing process as a system and investigating the interrelationships of system components enables a better understanding of the images. We present here a system model for the remote sensing process of CRISM images. Our results assist in understanding the effects of environmental and instrumental processes on the formation of CRISM images and will hopefully aid researchers in the planning and execution of scientific analysis using CRISM data.

The focus of this project is on interrelationships between the atmosphere, sensor noise, and scattered path radiance and their influence on detection accuracy of the mineral species. We create controlled scenarios with spectral features that are challenging to detect using manual and automatic techniques.

Image Creation: The reflected light that enters the input aperture of the sensing instrument experiences many interactions. Solar radiation passes through the atmosphere, where it is partially absorbed and scattered, before being absorbed or reflected by the Martian surface material. The reflected light then passes again through the atmosphere en route to the sensor.

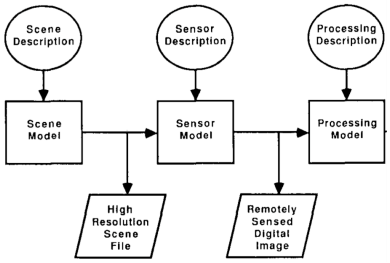

Fig. 1. Schematic representation of a remote sensing system (adapted from Kekeres et Landgrebe[1]).

The sensor samples the incoming optical energy spatially and spectrally producing a spectral scene characterization that is transmitted to the processing facility. Geometric and radiometric calibration is then performed on the image in order to compare the image to other data sets. Finally, the image undergoes an interpretation phase where information is retrieved about the surface composition. Fig. 1 represent a schematic view of the process as a system in which input data (ellipses) are fed into the model (rectangles) to produce simulation outputs.

Scene model: The scene model describes the scene and produces a high spatial and spectral resolution scene file consisting of the spectral radiance detected by the sensor. High spectral resolution means several spectral samples per sensor spectral band. The form of the scene model we have chosen combines a stochastic surface reflectance model with a deterministic solar and atmospheric model. Mineral endmembers are modeled by random vectors representing intrinsic spectral variability of a mineral due to composition, grain size and other effects. In this initial model we assume areal (linear) mixing of the endmembers. Mineral classes are defined from a single mineral or binary mixtures. These classes are mapped into different zones based on an altimetry map generated with fractals and are populated with an autoregressive random field, which determines the abundance of the endmember in a mixture of the spectral variation of a single class mineral. The atmospheric model is derived by first principles and is a trade-off between interpretability of the atmospheric parameters and realistic results. The atmospheric simulation program DISORT [2] computes the solar irradiance, skylight radiance, atmospheric transmittance and scattered path radiance to complete the scene model.

Sensor model: The sensor model transforms the scene spectral radiance file into a hyperspectral digital image of the scene. The model applies the spectral response by integrating each band's spectral response across the scene spectral range, and applies the spatial response of the sensor by integrating a separable point spread function in the two spatial dimensions [3].

Noise model: The artifacts and distortions typical of CRISM images have been briefly described by Parente [4]. Striping noise due to calibration errors is applied as a multiplicatively line-independent random process while spiking due to cosmic rays is modeled as a random process. This is correlated in the along track direction to model the persistency in time of elevated signal level in the event of a spike. Thermal noise is modeled as an independent Gaussian random process.

Processing model: We assume that the data are corrected for solar irradiance curve. We apply standard correction steps such as correction for the effect of the incidence angle and volcano-scan atmospheric correction [e.g. 5]. The model integrates an image-denoising algorithm [4]. and a tool for visualization of the data cloud in high dimensional space for the purpose of scene endmember extraction.

Application: We created a synthetic scene with 3 classes to illustrate this simulation process: a mixture of montmorillonite and altered volcanic material, a mixture of nontronite and altered volcanic material and

a small patch of kaolinite. We used lab reflectance spectra of such materials as a starting point. Fig. 2 shows the reflectance map with the spectral classes. The size of the image 200 by 200 pixels and the resolution is set at 10 m / pixel. The patch of Kaolinite is especially evident. Fig. 3 shows the relative spectra for the regions depicted in Fig. 2, in our simulation the spectral resolution is of 0.5 nm/channel. Noise is added initially to the laboratory spectra in order to simulate measurement uncertainty.

Fig. 2: Reflectance image with a 15x20 pixel kaolinite patch.

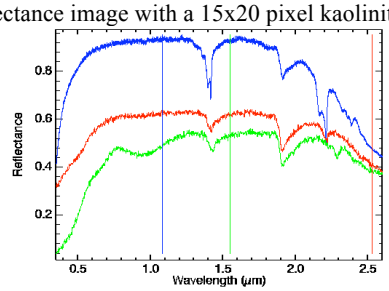

Fig. 3: Lab spectra of mineral plus synthetic noise. Blue: Pure kaolinite, Red: montmorillonite with altered volcanic material, Green: nontronite with altered volcanic material

The atmospheric module is then applied to the reflectance image assuming lambertian surfaces and with incidence angle and atmospheric transmission depending on the randomly generated altimetry map. Fig. 4 is an illustration of such process that produces at-sensor radiance. The result of the application of the sensor module and the subsequent atmospheric correction is depicted in Fig. 5. The sensor response reduces the spatial resolution to approximately 18 m/pixel and the spectral resolution to 6.55 nm/channel.

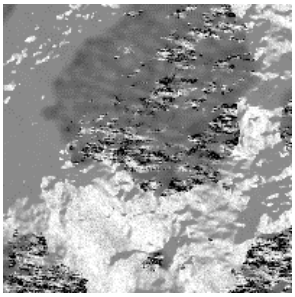

Fig. 4: Example of atmospheric and photometric contribution to the radiance.

Fig. 5 the effect of the spatial instrument integration (blurring) together with the striping and spiking noise. Also immediately evident from Fig. 5 is that the small patch of kaolinite is not noticeable even if we stretch the image in such a way to enhance subtle features. A confirmation of this fact comes from Fig. 6, which represents corresponding spectra from the scene in Fig. 5. Besides a loss of spectral resolution and spiking noise we notice that a typical spectrum from general coordinates corresponding to the kaolinite patch shows a possible mixture but no definitive kaolinite detection. A combination of scattering from adjacent montmorillonite pixels, linear mixing from the instrument function and noise is the cause of the uncertainty.

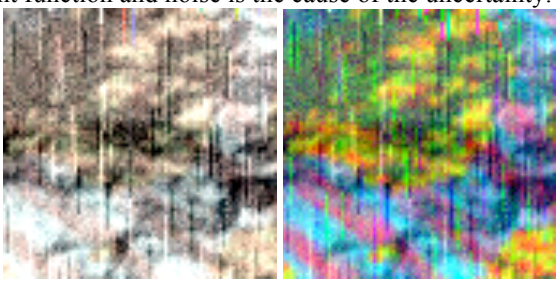

Fig. 5: (left) Fully processed image, convolved with the instrument function with noise and atmospheric correction. (Right) Fully processed image with decorrelation stretch.

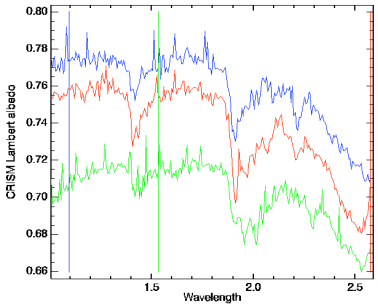

Fig. 6: Final mineral Detections in simulated image. Green: Nontronite, Red: Possible Threshold Kaolinite detection, Blue: Montmorillonite detection.

Conclusions: We presented a model and simulation of the image formation and treatment of CRISM images. The model includes sup-pixel mineral mixing, atmospheric contribution, sensor model and simple post-processing in order to produce an output comparable to a typical CRISM image. We presented an example of our system that created a scene with a small patch of kaolinite. The application of the simulation system allow the authors to record the difficult identification of the kaolinite patch both spectrally and spatially. Future experiments will test advanced detection algorithms for positive automated identification of mixture endmembers in such difficult scenarios based on the model here proposed.

References: [1] Kekeres J.P. and Landgrebe (1989) , *IEEE Transactions on Geoscience and Remote Sensing, 27,6, 762-761.* [2] McGuire P.C. et al. (2008) *IEEE Transactions on Geoscience and Remote Sensing, 46,* 4020-4040. [3] Schott J. R. (1997), Remote sensing. [4] Parente M. (2008) LPSC, #2528. [5] Mustard J. F. et al. (2008) *Nature, 454,* doi: 10.1038/nature07097, 305-309.